

FAINT WHITE DWARF FLUX STANDARDS: DATA AND MODELS

RALPH C. BOHLIN,¹ SUSANA DEUSTUA,² GAUTHAM NARAYAN,³ ABHIJIT SAHA,⁴
ANNALISA CALAMIDA,¹ KARL D. GORDON,¹ JAY B. HOLBERG,⁵ IVAN HUBENY,⁶
THOMAS MATHESON,⁴ AND ARMIN REST⁷

¹*Space Telescope Science Institute, 3700 San Martin Drive, Baltimore, MD 21218, USA*

²*Sensor Science Division, National Institute of Standards and Technology, Gaithersburg, MD 20899-8441, USA*

³*University of Illinois at Urbana-Champaign, 1002 W. Green Street, Urbana, IL 61801, USA*

⁴*NSF's National Optical Infrared Astronomy Research Laboratory, 950 North Cherry Avenue, Tucson, AZ 85719, USA*

⁵*The University of Arizona, Lunar and Planetary Laboratory, 1629 East University Boulevard, Tucson, AZ 85721, USA*

⁶*The University of Arizona, Steward Observatory, 933 North Cherry Avenue, Tucson, AZ 85721, USA*

⁷*Space Telescope Science Institute, 3700 San Martin Drive, Baltimore, MD 21218, USA and Department of Physics and Astronomy, Johns Hopkins University, Baltimore, MD 21218, USA*

ABSTRACT

Fainter standard stars are essential for the calibration of larger telescopes. This work adds to the CALSPEC (calibration spectra) database 19 faint white dwarfs (WDs) with all-sky coverage and V magnitudes between 16.5 and 18.7. Included for these stars is new UV (ultraviolet) HST (Hubble Space Telescope) STIS (Space Telescope Imaging Spectrometer) spectrophotometry between 1150 and 3000 Å with a resolution of ~500. Pure hydrogen WD models are fit to these UV spectra and to six-band HST/WFC3 (Wide Field Camera 3) photometry at 0.28 to 1.6 μm to construct predicted model SEDs (spectral energy distributions) covering wavelengths from 900 Å to the JWST (James Webb Space Telescope) limit of 30 μm using well-established CALSPEC procedures for producing flux standards with the goal of 1% accuracy.

Keywords: stars: atmospheres — stars: fundamental parameters — techniques: spectroscopic — infrared: stars

1. INTRODUCTION

Bohlin et al. (2020) and references therein discuss the CALSPEC¹ database of SEDs for stellar flux standards. The CALSPEC SEDs are based on HST/STIS flux calibrated spectra, sometimes supplemented by HST/WFC3 and HST NICMOS (Near Infrared Camera and Multi-Object Spectrometer) spectrophotometry. Model atmosphere grids of stellar spectra are fit to these measured flux distributions to estimate the flux at longer wavelengths than covered by the HST observations. For this work, the Hubeny grid version 207 is used to fit the STIS SEDs. Bohlin et al. (2020) introduced this grid², which contains 132 models with effective temperature (T_{eff}) in the range 20,000-95,000 K and

¹ <http://www.stsci.edu/hst/instrumentation/reference-data-for-calibration-and-tools/astronomical-catalogs/calspec>

² DOI10.17909/t9-7myn-4y46

surface gravity ($\log g$) between 7.0 and 9.5, with six steps of 0.5, where g has units of cm s^{-2} . The steps in T_{eff} are 2,000 K between 20,000 and 40,000 K and 5,000 K between 40,000 and 95,000 K.

The normal CALSPEC SED includes a mix of the observed spectrophotometry with model extrapolations to longer wavelengths. The fitted models provide standard star flux distributions for calibration of IR (infrared) instrumentation. Most of the current JWST CALSPEC standards are too bright ($V < 16$) for many of the standard detector modes and provide only indirect flux calibrations via subarray data. However, our new fainter stars ($V=16$ to 19) can be observed in the standard science modes, thus avoiding any uncertainty associated with the small detector subarray modes used for bright stars. The JWST flux calibration plan (Gordon et al. 2022) utilizes three categories of CALSPEC standards: hot, A type, and G type stars, while WDs fall in the hot star category.

Our long term project to establish a network of faint WD stars with complete sky coverage provides an ideal set of fainter IR flux standards for JWST. These faint star SEDs were based on HST/WFC3 photometry in six filters for 35 WDs from the A. Saha programs 12967, 13711, and 15113. Narayan et al. (2019) published preliminary results, while Calamida et al. (2022) present a variability analysis and finding charts. Details of the WFC3 photometric data reduction are in Calamida et al. (2019), which includes a description of the ILAPH photometry. Axelrod et al. (2023) fit this six-filter WFC3 photometry to sub-percent precision with pure-hydrogen model atmosphere SEDs using a hierarchical Bayesian analysis process similar to the preliminary analysis of Narayan et al. (2019).

The Axelrod et al. (2023) paper examines the internal consistency of the SEDs of all 35 DA white dwarfs that span a wide range of temperatures and surface gravities and includes the three primary WDs that are used to define the flux scale for CALSPEC. This analysis compares their measured fluxes from the near-UV to the near-IR against predictions from the Hubeny & Lanz (1995) NLTE (non-local thermodynamic equilibrium) models of DA white dwarf atmospheres and results in a rigid lattice of SEDs on a physical basis and in relative apparent brightness for the set of stars that is self-consistent to a few milli-mag rms within this wavelength domain. The method of analysis is independent of CALSPEC, except for effectively borrowing the zero-point used in the 2014 version of the CALSPEC (CALSPEC14) flux scale for the absolute flux of Vega at 5556 Å (air) to achromatically tie this 'lattice' to an absolute flux scale. While CALSPEC14 and Axelrod et al. (2023) both used the same three primary DA white dwarf model SEDs, the current implementation of CALSPEC differs in two respects: a) it is based on newer models, which extend the wavelength coverage to the JWST limit of 30 μm ; and b) its absolute fluxes reconcile absolute flux measures of Sirius in the midIR with the Vega 5556 Å flux to determine the achromatic flux zero-point. The analysis in this paper is tied to the current Bohlin et al. (2020) CALSPEC flux scale and, thus, can differ systematically from that derived in Axelrod et al. (2023). In addition, the fitted data sets and methods of analyses differ.

To supplement the WFC3 photometric constraints on the model fits, the HST program 16764 (G. Narayan PI) obtained shorter wavelength coverage with the STIS G140L and G230L gratings for 19 of the 32 stars in Axelrod et al. (2023) that are bright enough to obtain STIS UV spectrophotometry between 1150 and 3000 Å. Our goal is to produce CALSPEC SEDs extending to the JWST limit of 30 μm by fitting both the original WFC3 photometry along with the new STIS spectrophotometry. Consequent to the statements in the above paragraph, minor updates bring the Axelrod photometry onto the current CALSPEC flux scale system; and more recent NLTE models extend the wavelength coverage to 30 μm .

An analysis with the standard χ^2 technique of [Bohlin et al. \(2020\)](#) used for all the current CALSPEC models provides consistent SEDs for on-going JWST flux calibrations with fainter standards than are currently available. JWST results will provide feedback to our continuing analyses that update these preliminary results. The definition of flux standards is never finalized but is a continually evolving process of improvement as the data set and analysis techniques mature.

Section 2 describes the HST data, while Section 3 explains the procedure of finding the models that best fit the data. Section 4 summarizes the results and the future plans for improvements.

2. HST DATA REDUCTION

2.1. STIS

The STIS spectra are extracted from the raw STIS images using a custom set of software provided by the original STIS Instrument Definition Team and Don Lindler. The advantages of custom software over the STScI pipeline products include automatic repair of hot pixels, optimization of cosmic ray rejection, editing of residual noise spikes, wider extraction heights to improve CCD photometric precision, co-addition of multiple observations, merging of the separate grating spectra into one complete SED, and correction of any small offsets from the wavelengths defined by the STIS emission line calibration spectra. In addition, every new monitor observation (about three times per year) of the MAMA standard GRW+70 °5824 or the CCD standard AGK+81°266 results in a complete updated flux calibration ([Bohlin et al. 2020](#)) that accounts for the changes in instrumental sensitivity and is applicable to all of the CALSPEC stars. IDL and Python versions of these STIS analysis routines reside in Github³.

2.2. WFC3

In addition to the UV STIS spectrophotometry, the WFC3 photometry in six filters constrains the model fits over the wavelength range from the near-UV to the IR filter F160W at a pivot wavelength of 15369 Å. The [Axelrod et al. \(2023\)](#) 32 SEDs have absolute fluxes defined by the three CALSPEC *mod_010.fits SEDs for the three primary WDs, G191B2B, GD153, and GD71, on the flux scale of [Bohlin et al. \(2014\)](#), which was current for the original analysis of [Narayan et al. \(2019\)](#), while the present HST flux scale is defined by the three *mod_012.fits SEDs of [Bohlin et al. \(2020\)](#). These three CALSPEC SEDs for the primary WDs provide the defining basis for all of the HST flux calibrations, including both STIS spectrophotometry and WFC3 photometry.

Thus, the transformation of the [Axelrod et al. \(2023\)](#) 2014 absolute photometry to the current 2020 flux scale is just the average ratios of the synthetic photometry for the three 2020 *mod_012.fits SEDs to the synthetic photometry of the 2014 *mod_010.fits SEDs, as presented in Table 1. As explained in detail in [Bohlin et al. \(2020\)](#), the transformation from the 2014 to the 2020 flux has an absolute gray flux increase of 0.87% and a wavelength dependent change due to the improved models for the three stars. The combination of these two updates total to <2% and bring the [Axelrod et al. \(2023\)](#) photometry from the 2014 to the current 2020 HST photometric scale of Table 2. [Axelrod et al. \(2023\)](#) provides both the original WFC3 photometry and a corrected version updated for any WFC3 flux calibration errors, such as poor bandpass transmission functions. To use the corrected values, the bandpass transmission must also be corrected to maintain consistency between the corrected photometry and the synthetic photometry. Here, the analysis begins with the original photometry,

³ <https://github.com/spacetelescope/ABSCAL>

in order to avoid questions of the true bandpass and to compare any systematic WFC3 photometry residuals with those same residuals found by Axelrod.

The STIS G230L grating covers the same wavelengths as the WFC3 F275W filter; and the synthetic STIS F275W photometry is close to the original WFC3 photometry, which testifies to the precision of our WFC3 effective fluxes. On average, the original Axelrod WFC3 photometry is 0.003 mag fainter than the STIS synthetic photometry; and the rms difference between the synthetic and actual photometry is 0.006 mag for our 19 WDs, which is consistent with the STIS G230L broadband repeatability of 0.002–0.003 mag (Bohlin et al. 2019) for brighter stars.

3. RESULT FROM FITTING MODELS

To extend the flux distributions to longer and shorter wavelengths, model atmosphere SEDs are fit to the STIS and WFC3 data with the reduced χ^2 technique and the Hubeny TLUSTY pure hydrogen models in the standard CALSPEC style (Bohlin et al. 2020). To find the best fit model, the WFC3 photometry is compared to synthetic photometry for the model SED; and the STIS data are fit in bins that avoid the often strong interstellar lines and regions with weak signal and high photon noise. Table 3 lists these wavelength bins. The model fitting finds the smallest χ^2 (Bohlin et al. 2017; Bohlin & Deustua 2019; Bohlin et al. 2020) by varying T_{eff} and E(B-V), which are the model effective temperature and selective extinction.

3.1. Details of the χ^2 Fitting

The models from the Hubeny TLUSTY grid are compared to the STIS observations in the wavelength bins in Table 3, and synthetic photometry of the models is compared to the actual WFC3 photometry using error estimates for STIS, WFC3, and the models to form the χ^2 sums. Modeling uncertainties are proportional to the amount of line-blanketing in each STIS bin or in each WFC3 bandpass. The best fit is found by varying the T_{eff} and E(B-V) to find the minimum of the reduced χ^2 value that defines the model. The mesh size of the model search parameters are 10 K in T_{eff} and 0.001 in E(B-V). Our analysis does not consider the constraints of the ground-based Balmer spectra on the surface gravity ($\log g$), while Axelrod does utilize the Balmer lines. The pressure broadened Balmer line profiles are most sensitive to $\log g$; and therefore, the Axelrod $\log g$ values are used and not varied in the fitting. An example of the model fitting appears in Figure 1 for WDFS1434-28 with the noisy STIS G140L data shown in red in the bottom two panels.

The χ^2 technique relies on minimizing the sum of the squares of the ratio of the residual differences of the data from the model, as divided by the uncertainty estimates. The wide STIS bands used for fitting the model minimize the uncertainty from photon noise. The WFC3 rms photometric repeatabilities are 0.3% for the five UVIS filters and 0.6% for F160W (Axelrod et al. 2023). For STIS, the repeatability as a function of wavelength for the monitor star GRW+70 °5824 is of order 0.7% for G140L and 0.3% for G230L (Bohlin et al. 2019). In addition, the STIS background uncertainty is 4% of the sky background level to account for the large separation of the background regions from the spectral trace. The two uncertainties are combined in quadrature for each STIS bin; and the relative weights of each STIS bin and WFC3 photometry point are their individual χ^2 values, which are then all combined in quadrature to get the total χ^2 . The minimum total χ^2 defines the T_{eff} and

Table 1. 2020 vs. 2014 Effective Flux

Star	Filter	2014 ^a	2020 ^a	Ratio
G191B2B	F275W	9.4780e-13	9.6486e-13	1.0180
GD153	F275W	1.9550e-13	1.9967e-13	1.0213
GD71	F275W	2.3789e-13	2.4361e-13	1.0240
AVERAGE				1.02112
G191B2B	F336W	4.2643e-13	4.3315e-13	1.0158
GD153	F336W	9.0853e-14	9.2391e-14	1.0169
GD71	F336W	1.1254e-13	1.1475e-13	1.0196
AVERAGE				1.01742
G191B2B	F475W	1.1991e-13	1.2133e-13	1.0119
GD153	F475W	2.7642e-14	2.7878e-14	1.0085
GD71	F475W	3.6412e-14	3.6824e-14	1.0113
AVERAGE				1.01058
G191B2B	F625W	4.3035e-14	4.3423e-14	1.0090
GD153	F625W	1.0194e-14	1.0245e-14	1.0050
GD71	F625W	1.3687e-14	1.3785e-14	1.0072
AVERAGE				1.00708
G191B2B	F775W	1.9553e-14	1.9680e-14	1.0065
GD153	F775W	4.6757e-15	4.6946e-15	1.0040
GD71	F775W	6.3272e-15	6.3650e-15	1.0060
AVERAGE				1.00551
G191B2B	F160W	1.2958e-15	1.2935e-15	0.9982
GD153	F160W	3.1516e-16	3.1571e-16	1.0017
GD71	F160W	4.3410e-16	4.3540e-16	1.0030
AVERAGE				1.00097

^a $\text{erg s}^{-1} \text{cm}^{-2} \text{\AA}^{-1}$

NOTE—Synthetic absolute effective fluxes for the three primary WD stars in six WFC3 filters as computed from their 2014 CALSPEC SEDs (*mod_010.fits) and the 2020 SEDs (*mod_012.fits). The average ratio of the 2020 to the 2014 fluxes defines the six updates required to convert all of the [Axelrod et al. \(2023\)](#) photometry to the current 2020 CALSPEC flux scale.

Table 2. 2020 WFC3 AB magnitudes

Star	F275W	F336W	F475W	F625W	F775W	F160W
G191B2B	10.467	10.871	11.488	12.023	12.445	13.884
GD153	12.179	12.549	13.089	13.590	13.996	15.413
GD71	11.966	12.317	12.788	13.271	13.666	15.067
WDFS0103-00	18.172	18.508	19.072	19.561	19.959	21.354
WDFS0122-30	17.648	17.975	18.449	18.914	19.314	20.704
WDFS0228-08	19.495	19.696	19.804	20.161	20.495	21.736
WDFS0238-36	17.767	17.953	18.084	18.431	18.751	19.991
WDFS0248+33	17.806	18.021	18.359	18.738	19.071	20.339
WDFS0458-56	17.000	17.332	17.743	18.209	18.595	19.998
WDFS0541-19	17.998	18.196	18.265	18.616	18.954	20.193
WDFS0639-57	17.299	17.634	18.167	18.631	19.011	20.379
WDFS0727+32	17.141	17.452	17.982	18.449	18.831	20.216
WDFS0815+07	18.927	19.245	19.705	20.176	20.573	21.961
WDFS0956-38	17.675	17.840	17.851	18.171	18.491	19.689
WDFS1024-00	18.238	18.495	18.893	19.309	19.659	20.990
WDFS1055-36	17.347	17.634	18.002	18.419	18.787	20.134
WDFS1110-17	17.018	17.335	17.856	18.306	18.683	20.056
WDFS1111+39	17.420	17.811	18.410	18.931	19.338	20.796
WDFS1206+02	18.217	18.470	18.661	19.052	19.405	20.702
WDFS1206-27	15.714	16.022	16.465	16.915	17.287	18.648
WDFS1214+45	16.917	17.264	17.750	18.228	18.623	20.037
WDFS1302+10	16.165	16.503	17.025	17.506	17.898	19.302
WDFS1314-03	18.235	18.578	19.091	19.559	19.949	21.327
WDFS1434-28	17.815	17.958	17.957	18.277	18.578	19.758
WDFS1514+00	15.087	15.372	15.698	16.112	16.465	17.786
WDFS1535-77	15.576	15.950	16.542	17.042	17.451	18.889
WDFS1557+55	16.477	16.858	17.459	17.984	18.382	19.833
WDFS1638+00	17.993	18.299	18.829	19.273	19.654	20.995
WDFS1814+78	15.768	16.102	16.533	16.998	17.387	18.785
WDFS1837-70	17.619	17.772	17.759	18.084	18.405	19.605
WDFS1930-52	16.706	17.015	17.473	17.919	18.295	19.654
WDFS2101-05	18.045	18.315	18.645	19.056	19.408	20.739
WDFS2317-29	17.874	18.122	18.338	18.740	19.100	20.422
WDFS2329+00	17.920	18.090	18.150	18.462	18.769	19.994
WDFS2351+37	17.426	17.643	18.064	18.451	18.781	20.074

NOTE—WFC3 photometry on the 2020 CALSPEC flux scale. The Table 1 corrections convert the original WFC3 photometry from the table 1 [Axelrod et al. \(2023\)](#) 2014 flux scale to the current 2020 scale.

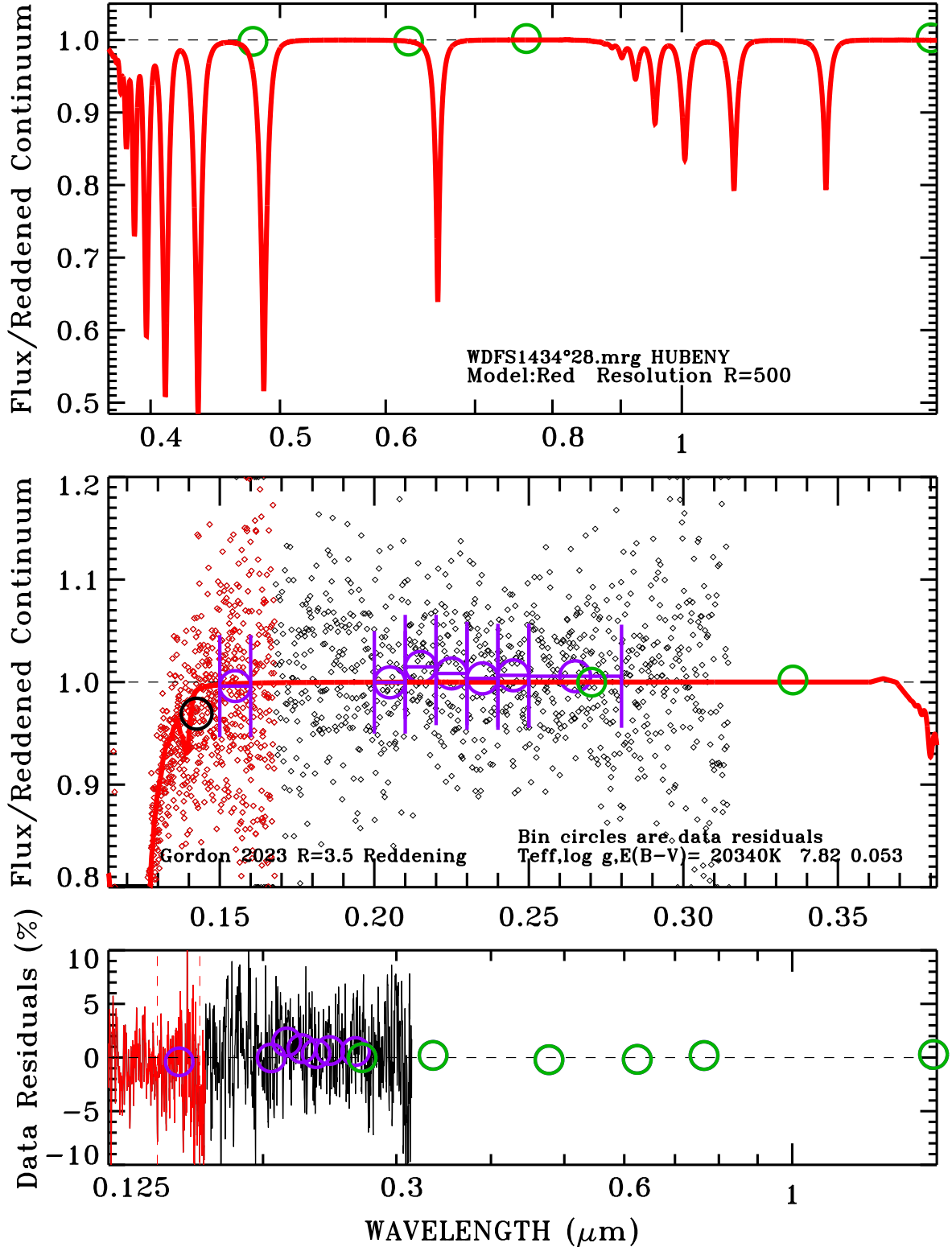


Figure 1. Model fit and residuals for WDFS1434-28 with the parameters from Table 4 written on the plot. The heavy red line in the top two panels represents the model divided by its continuum to flatten the display and preserve spectral features, while in all three panels the residuals are large green circles for the WFC3 photometry, large purple circles for the useful STIS bins, and a large black circle for the STIS G140L bin that is not used as a constraint to the fit. Middle panel: Small diamonds are STIS data for G140 (red) and G230L (black). The dip in the model near 1400 Å is a quasi-molecular hydrogen feature. Bottom panel: The purple bars that indicate the bin width and the black circle are omitted for clarity. The red and black STIS data are binned to a resolution $R = 500$.

Table 3. Broad Bands for Fitting WD Models

Wavelength Ranges (\AA)							
1350–1500 ^a	1500–1600	2000–2100 ^b	2100–2200 ^b	2200–2300 ^b	2300–2400 ^b	2400–2500 ^b	2500–2800 ^c

^aNot used for four of the coolest stars WDFS0956-38, WDFS1434-28, WDFS1837-70, and WDFS2317-29 because of confusion with the strong quasi-molecular hydrogen feature near 1 in the Hubeny models.

^bNot used for WDFS1514+00 and WDFS2351+37, because the 2175 \AA extinction bump is anomalously strong and cannot be fit with any of the [Gordon et al. \(2023\)](#) average extinction curves

^cReplaced by 2500–3100 for WDFS1514+00 and WDFS2351+37 that have very strong extinction

E(B-V) of the best fitting SED for each WD. To ensure finding the global minimum and not a local minimum χ^2 , the process is iterated to convergence with perturbations of 30K in T_{eff} .

3.2. Extinction by Interstellar Dust

The proper accounting for extinction from interstellar dust is crucial to precisely fitting measured SEDs to theoretical models, which are unextinguished. If A(V) is the total extinction in magnitude units from interstellar dust in the V band and the selective extinction E(B-V) is defined as A(B)-A(V) where A(B) is the extinction in the B band, then average extinction curves are specified in terms of the parameter R(V)=A(V)/E(B-V). Here, the default is R(V)=3.1, which is the average over the sky that is also adopted by [Axelrod et al. \(2023\)](#). The average extinction prescriptions for R(V) are from [Gordon et al. \(2023\)](#), but there are frequent deviations from these averages for individual sightlines ([Witt et al. 1984](#); [Mathis & Cardelli 1992](#); [Valencic et al. 2004](#); [Gordon et al. 2023](#)).

The larger the extinction A(V), the larger the effect on the observed SED; and the extinction is somewhat degenerate with T_{eff} in the sense that larger A(V) and lower T_{eff} both reduce the UV flux with respect to longer wavelengths. The extended wavelength coverage with the new STIS data reduces the degeneracy in comparison to the smaller wavelength range of just the WFC3 data alone.

For four stars with some of the higher extinctions in Table 4, exceptions to R(V)=3.1 are required, in order to bring the residuals to $\lesssim 1\%$ for all STIS bins and all WFC3 photometry. Because these larger values of A(V) have the biggest effect on the observed SED, deviations from the default R(V)=3.1 can significantly change the quality of the model fits. For example for WDFS0639-57, the worst WFC3 residual is for F160W, which drops from 2.8% to 0.3%; and the overall χ^2 of the fit decreases from 7.7 to 2.0 for the fits with R(V)=3.1 vs. R(V)=4.2.

For many stars, fitting the G140L data is not possible, even if the restriction of R(V)=3.1 is relaxed. Thus, the model fitting for these 12 stars proceeds by omitting the two G140L bins. Because the G140L flux is mostly lower than the model fit to the longer wavelength data, random photometric repeatability for our faint stars seems an unlikely culprit. For the 12 stars where G140L is not a constraint, the average G140L residuals in the final column of Table 4 are often many sigma when compared to the $\approx 1\%$ repeatability for the STIS monitor star GRW+70 °5824. These residuals are with respect to the model fitted to the remaining STIS and WFC3 data after omission of the two G140L bins. Other possibilities for the poor fits to G140L include (a) faint cooler sources within

Table 4. Model parameters

Star	Teff (K)	log g	A(V)	R(V)	G140L Resid (%)
WDFS0122-30	34150	7.77	0.043	3.1	-4.7
WDFS0248+33	33230	7.10	0.323	3.4	...
WDFS0458-56	30290	7.79	0.009	3.1	...
WDFS0639-57	53230	7.90	0.189	4.2	-4.5
WDFS0956-38	20100	7.88	0.112	3.1	...
WDFS1055-36	29570	7.93	0.093	3.1	-3.6
WDFS1110-17	46700	8.01	0.146	3.1	-4.2
WDFS1206-27	33980	7.90	0.099	3.1	-1.6
WDFS1214+45	34170	7.85	0.003	3.1	-2.0
WDFS1302+10	42090	7.93	0.074	3.1	-7.8
WDFS1434-28	20340	7.82	0.185	3.5	...
WDFS1514+00	29200	7.90	0.121	3.1	+4.3
WDFS1535-77	49940	9.08	0.012	3.1	-2.7
WDFS1557+55	57830	7.55	0.012	3.1	-2.3
WDFS1814+78	31040	7.80	0.006	3.1	-2.3
WDFS1837-70	19810	7.87	0.105	3.1	...
WDFS1930-52	36300	7.67	0.133	3.5	...
WDFS2317-29	24030	7.85	0.022	3.1	...
WDFS2351+37	41290	7.70	0.313	3.1	+5.4

$\sim 0.5''$ that contribute a few percent to the longer wavelengths but not to the FUV G140L signal or (b) heavy FUV metal line-blanketing, as is the case for G191B2B, but which has only $\approx 1\%$ FUV blanketing.

Perhaps, the most likely reason for poor fits is that the reddening is anomalous and does not correspond to any average extinction curve. [Gordon et al. \(2023\)](#) show considerable scatter in $A(\lambda)/A(V)$ at $\lambda=1500 \text{ \AA}$ and $R(V)$ near 3.1. Figure 2 illustrates the worst case residuals for WDFS2351+37 that cannot be fit by any [Gordon et al. \(2023\)](#) average extinction. The fit is only to the data longward of 2500 \AA , and the omitted short wavelength STIS bins appear as open black circles. In the middle and lower panels, the red model lies above the flux in the 2175 \AA extinction bump and below the G140L STIS data, which suggests that the extinction is anomalously low in the 1500 \AA region compared to a stronger than average 2175 \AA extinction bump. Similarly, WDFS1514+00 also has a positive G140L residual in Table 4. No average dust extinction curve of [Gordon et al. \(2023\)](#) provides a good fit to the observed ultraviolet SED of these two stars.

The most reliable model flux extrapolations in the IR to $32 \mu\text{m}$ are for the seven stars with models that do fit the G140L STIS data and, thus, have no entry in the G140L Residual column of Table 4.

Fig. Set 3. Model fit and residuals for the other 17 WDs

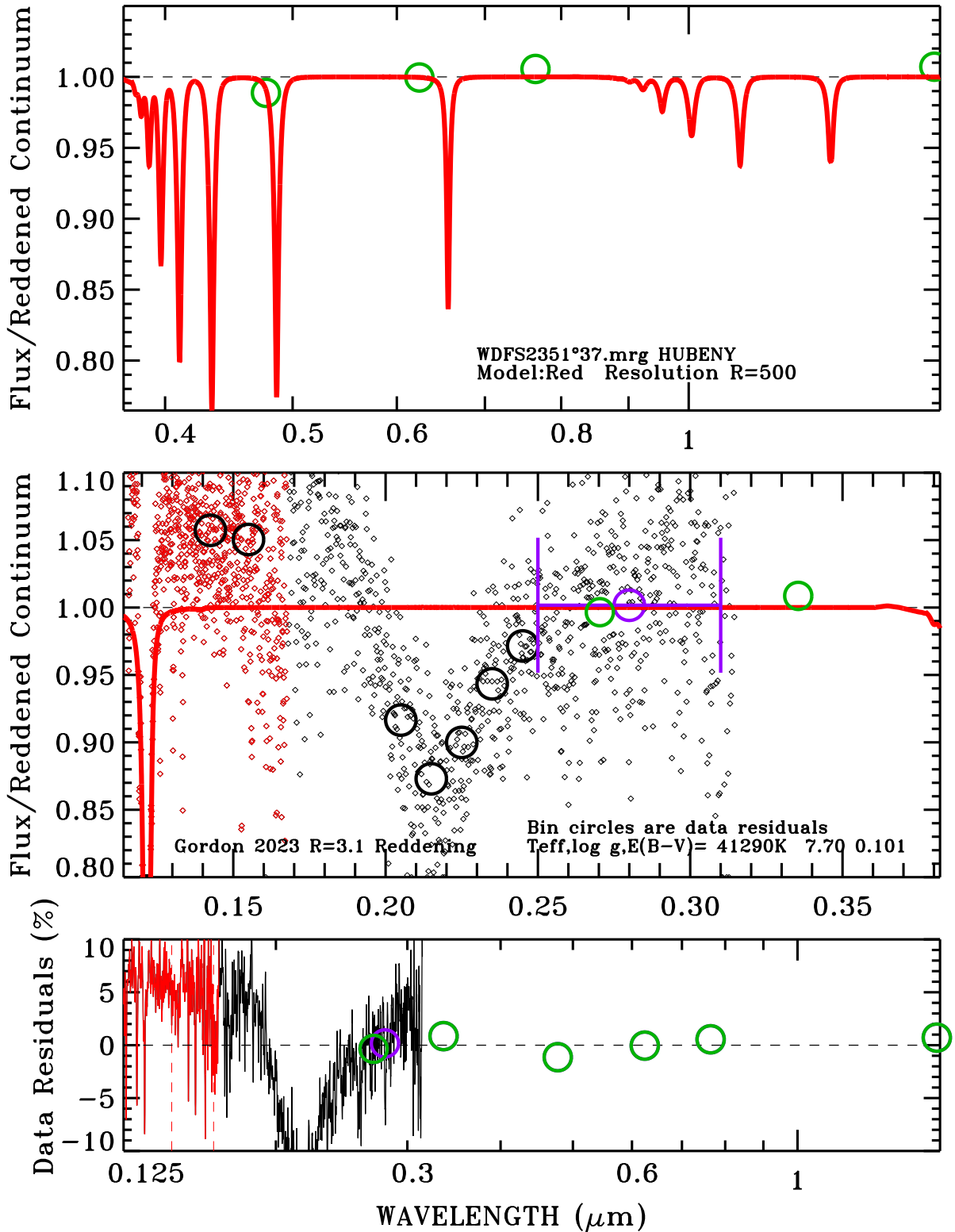


Figure 2. Model fit and residuals for WDFS2351+37 as in Figure 1. Seven STIS bins (large black circles) are omitted as constraints to the model fitting. The bottom panel shows the large STIS spectral residuals and the small residuals for the WFC3 photometry (green circles). The full figure set for the 17 WDs, beside Figure 1 and Figure 2, is available in the electronic version of this paper. [editor: please put the link to the Fig set here.]

Table 5.
Average WFC3 Offsets from the Model and
their Uncertainties in Mag Units

Filter	Avg	Uncert.
F275W	+0.001	0.006
F336W	-0.002	0.006
F475W	+0.006	0.004
F625W	-0.001	0.003
F775W	-0.002	0.003
F160W	-0.003	0.006

3.3. Statistics of the Fits

Table 5 contains the average offsets and their uncertainties of the deviation of the WFC3 photometry from the synthetic photometry for the 19 fitted models. The uncertainties, i.e. errors-in-the-mean, for the offsets are the rms values divided by $\sqrt{19}$. These results are consistent with the [Axelrod et al. \(2023\)](#) corrections to the original WFC3 photometry, except for slightly larger uncertainties.

3.4. SED Uncertainties

The Hubeny model atmosphere grid is compared to the similar Rauch grid ([Bohlin et al. 2020](#)) to verify their near equivalence and provide a lower limit to uncertainty of our final Hubeny SEDs. The Rauch TMAP models are nearly identical to the Hubeny TLUSTY models, except for the quasi-molecular hydrogen FUV absorption features in the TLUSTY models ([Bohlin et al. 2020](#)). Model fits with the TLUSTY or TMAP grids are generally within 1% of agreement. An outlier is WDFS0248+33, where the Rauch fit is 2% brighter than Hubeny at 30 μm . In the range of STIS and WFC3 observational constraints, the Table 4 model fits and the [Axelrod et al. \(2023\)](#) SEDs agree to 1%; but in the mid-IR, a minimum uncertainty is the 2% set by the worst agreement between the fits for the two independent grids. However, the actual errors in the IR can be larger, if noise or some systematic affects both the TLUSTY and TMAP fits similarly.

The best measure of uncertainty in the important CALSPEC extrapolations past the long wavelength constraint of F160W with a pivot wavelength of 15369 \AA is defined by how well the current brighter standards work for JWST preliminary flux calibrations. The presently limited set of CALSPEC SEDs are derived from fitting HST flux measures with the same χ^2 technique used here. These preliminary JWST flux calibrations are generally consistent in the 2–30 μm range to better than $\approx 3\%$ ([Gordon et al. 2024](#), submitted). At shorter wavelengths in the 0.27 to 1.6 μm range with WFC3 photometry, an uncertainty of $\approx 1\%$ is demonstrated by that level of agreement with the seminal results of [Axelrod et al. \(2023\)](#).

4. DISCUSSION

Our model fits to the HST STIS spectroscopic plus WFC3 photometric observations provide continuous wavelength coverage from 900 \AA to 30 μm at a resolution $R=5,000$. The mid-IR flux dis-

tributions to 30 μm are essential for the flux calibration of the JWST instruments. Consistency of the JWST instrumental calibrations from our WDs in comparison to results for A and G type stars would validate our WD model extrapolations into the mid-IR.

While our results will be refined by on-going studies, the present results build on the comprehensive [Axelrod et al. \(2023\)](#) work and are adequate for an initial delivery to CALSPEC⁴, in order to provide our all-sky network of faint flux standards for calibration of JWST and other large-aperture facilities such as Euclid, the Nancy Grace Roman Telescope, and the Vera C. Rubin Observatory. With the new STIS data, NLTE models with wavelength coverage to 30 μm , and SEDs on the current HST CALSPEC flux scale, our updated SEDs are immediately useful. Future revisions will be posted, as is the usual custom for CALSPEC quality SEDs, which track on-going improvements to the data reduction and to the model fitting techniques.

The HST data presented in this article were obtained from the Mikulski Archive for Space Telescopes (MAST) at the Space Telescope Science Institute. The specific observations analyzed can be accessed via [10.17909/bwd3-9z83](https://archive.stsci.edu/hst/instrumentation/reference-data-hub/).

ACKNOWLEDGEMENTS

Support for this work was provided by NASA through the Space Telescope Science Institute, which is operated by AURA, Inc., under NASA contract NAS5-26555.

ORCID IDs

Ralph C. Bohlin <https://orcid.org/0000-0001-9806-0551>
 Abhijit Saha <https://orcid.org/0000-0002-6839-4881>
 Gautham Narayan <https://orcid.org/0000-0001-6022-0484>
 Annalisa Calamida <https://orcid.org/0000-0002-0882-7702>
 Susana Deustua <https://orcid.org/0000-0003-2823-360X>
 Karl D. Gordon <https://orcid.org/0000-0001-5340-6774>
 Jay B. Holberg <https://orcid.org/0000-0003-3082-0774>
 Ivan Hubenby <https://orcid.org/0000-0001-8816-236X>
 Thomas Matheson <https://orcid.org/0000-0001-6685-0479>
 Armin Rest <https://orcid.org/0000-0002-4410-5387>

REFERENCES

- Axelrod, T., Saha, A., Matheson, T., et al. 2023, *ApJ*, 951, 78
 Bohlin, R. C., & Deustua, S. E. 2019, *AJ*, 157, 229
 Bohlin, R. C., Deustua, S. E., & de Rosa, G. 2019, *The Astronomical Journal*, 158, 211
 Bohlin, R. C., Gordon, K. D., & Tremblay, P.-E. 2014, *PASP*, 126, 711
 Bohlin, R. C., Hubenby, I., & Rauch, T. 2020, *AJ*, 160, 21
 Bohlin, R. C., Mészáros, S., Fleming, S. W., et al. 2017, *AJ*, 153, 234
 Calamida, A., Matheson, T., Saha, A., et al. 2019, *ApJ*, 872, 199
 Calamida, A., Matheson, T., Olszewski, E. W., et al. 2022, *ApJ*, 940, 19
 Gordon, K. D., Clayton, G. C., Declair, M., et al. 2023, *ApJ*, 950, 86
 Gordon, K. D., Bohlin, R., Sloan, G. C., et al. 2022, *AJ*, 163, 267

⁴ <http://www.stsci.edu/hst/instrumentation/reference-data-hub/> Hubenby, I., & Lutz, E. 2022, *ApJ*, 930, 1075

Mathis, J. S., & Cardelli, J. A. 1992, ApJ, 398,
610

Narayan, G., Matheson, T., Saha, A., et al. 2019,
ApJS, 241, 20

Valencic, L. A., Clayton, G. C., & Gordon, K. D.
2004, ApJ, 616, 912

Witt, A. N., Bohlin, R. C., & Stecher, T. P. 1984,
ApJ, 279, 698